Arabian Journal of Chemistry (2022) **15**, 104270

King Saud University

Arabian Journal of Chemistry

www.ksu.edu.sa
www.sciencedirect.com

ORIGINAL ARTICLE

In vitro and *in vivo* evaluations of nanofibrous nanocomposite based on carboxymethyl cellulose/ polycaprolactone/cobalt-doped hydroxyapatite as the wound dressing materials

Yan Wang [a], **Dewang Shi** [b,*]

[a] *Department of Ophthalmology, Wenling First People's Hospital, Wenling 317500, China*
[b] *Department of Nursing, Zaozhuan Hospital, Zaozhuang 277100, China*

Received 30 November 2021; accepted 12 September 2022
Available online 17 September 2022

KEYWORDS

Wound healing;
Nanfibrous nanocomposites;
Cobalt;
Hydroxyapatite, Carboxymethyl cellulose

Abstract These days, Ophthalmic wound treatment is a major problem; due to its nature, bio/materials are the best choices as wound dressing materials. The main objective of the current survey is to develop and investigate effective wound dressing materials for skin care applications. In these ways, we combined the good biological properties of Cobalt-doped hydroxyapatite particles (CoHAp) with the structural properties of Polycaprolactone (PCL)/ carboxymethyl cellulose (CMC) nanofibers. Electrospinning and co-precipitation methods were used to synthesize nanofibers and CoHAp particles, respectively. Nanocomposites were synthesized in the absence and different percentages of CoHAp. The PCL/CMC, PCL/CMC/CoHA 5 %, PCL/CMC/CoHA 10 %, and PCL/CMC/CoHA 15 % formulated nanocomposites have the diameter of 383 ± 50, 391 ± 84, 441 ± 65, and 495 ± 99 nm, respectively. The synthesized nanofibrous wound dressing porosity and water absorption capacity were in the range of 40 to 60 % and 32 to 63 %, respectively. Hemo and cytocompatibility of the nanofibrous wound dressing were analyzed by in vitro evaluation, and the results were satisfactory and the structures were fully biocompatible. The PCL/CMC/CoHA 10 % wound dressing, were selected as the best nanocomposites for wound healing based on our animal studies on the healing outcomes. The results showed that the PCL/CMC nanofibers-Cobalt-doped HAp wound dressing is an effective bioactive nano-biomaterials for the wound healing process.

© 2022 The Author(s). Published by Elsevier B.V. on behalf of King Saud University. This is an open access article under the CC BY-NC-ND license (http://creativecommons.org/licenses/by-nc-nd/4.0/).

* Corresponding author at: No. 147, Longtou Middle Road, Shizhong District, Zaozhuang 277100, Shandong Province, China.
E-mail address: Dewang.shi@yahoo.com (D. Shi).

Peer review under responsibility of King Saud University.

Production and hosting by Elsevier

https://doi.org/10.1016/j.arabjc.2022.104270
1878-5352 © 2022 The Author(s). Published by Elsevier B.V. on behalf of King Saud University.
This is an open access article under the CC BY-NC-ND license (http://creativecommons.org/licenses/by-nc-nd/4.0/).

1. Introduction

Skin is the largest organ in the body and has vital functions ranging from protection against microorganism invasion and dehydration to vitamin D production and sensory functions, especially in the skin around the eyes. Accordingly, any damage to the skin should be treated appropriately. Wound healing is a complicated and multistage process involving different cells, stimuli, and signals (Venus et al., 2010; Rawat et al., 2016). Hemostasis, inflammation, proliferation, and maturation phases are the stages that progress sequentially. In normal conditions, minor skin wounds can heal can heal alone, but in large wounds and in unhealthy situations, such as diabetes, the healing goes complicated. In this situation, proper wound dressings must help the healing process (Hosgood, 2006; Braiman-Wiksman, 2007). Wound dressings are biomaterials primarily designed to protect the wound bed from microorganisms and dehydration, called passive dressings. These structures do not interact with skin components and wound healing elements. The next generation of wound dressings is bioactive and can interact with wound healing elements. These structures are called interactive dressings (Yusof, 2003; Maver, 2015; Unnithan, 2012).

The interactive wound dressings met the basic requirements of passive dressings, such as protection against microorganism invasion and body dehydration through the damaged skin. Moreover, the interactive wound dressings contain bioactive components designed to adjust one or more phases of wound healing. Various interactive wound dressings have been developed based on natural and synthetic substances. For instance, semipermeable films, hydroactives, hydrocolloids, foams, alginates, hydrogels, hydrofibers, and nanofibers (Han, 2016; Weller and Sussman, 2006; Abdelrahman and Newton, 2011; Asadi, 2021; Mohammadi, 2019). Among them, nanofibrous interactive wound dressings have attracted significant attention due to their fascinating properties. They have a large surface-to-volume ratio suitable for drug/bioactive molecules loading, adjustable porosity, and pore size providing oxygen exchange and preventing microorganisms' penetration and controlled vapor transmission. Electrospinning is a sophisticated nano/microfibers fabricating technique able to fabricate nano/microfibers with different morphology and architecture from a wide range of natural, synthetic, and semi-synthetic polymers. Moreover, solution-based electrospinning is compatible with various drugs, proteins, and other susceptible therapeutic agents, which makes the electrospinning technique favorable for biomedical applications.

Bioceramics, such as bioglass, β-calcium phosphate ceramics, and hydroxyapatite (HA), have shown promising results in the regeneration of hard tissues (Raisi, 2020; Doozandeh et al., 2020; Farazin, 2021; Beladi et al., 2017; Saber-Samandari, 2018). Recent studies indicated their application in soft tissue engineering applications. HA crystals can improve the scaffold's mechanical strength (to some extent) and the scaffold's biocompatibility, as well as serve as a reservoir for calcium and phosphate ions. It has been shown that calcium has vital roles in keratinocyte differentiation, proliferation, and normal hemostasis of the skin (Lansdown, 2002; Kawai, 2011; Magee et al., 1987). Several studies reported the modulatory effect of local calcium on skin cell proliferation, maturation and motility, and epidermal lipid barrier function, which are necessary for epidermal regeneration and dermal reconstruction in the skin wound healing process (Dlugosz and Yuspa, 1994; Lee, 1998; Trump, 1984). These studies confirmed the positive effects of incorporating HA crystals in the wound dressing materials. Moreover, it is possible to dope HA with different elements influencing wound healing process. The incorporation of inorganic ions into the scaffolds has been increased due to their low cost, clinical safety, and proper stability.

It has been reported that the application of Fe, Sr, Zn, Cu, St, and Co has b has beneficial effects on healing process, for instance Co can promote angiogenesis and improves the healing process. The biocompatibility of cobalt reported by several studies (Ansari, 2018; Klein, 2018; Lickmichand, 2019). Studies showed that strontium enhanced the release of angiogenic factors, such as matrix metalloproteinase-2 (MMP2), vascular endothelial growth factor (VEGF), and basic fibroblast growth factor (bFGF) (Rajalekshmy and Rekha, 2021). Accordingly, in the present study, we synthesized cobalt-doped HA crystal as the bioactive healing agent and incorporated the fabricated crystals in a CMC/PCL-based nanofibrous wound dressing.

2. Materials and methods

2.1. Reagents and chemicals

Polycaprolactone (PCL, MW: 80,000 g/mol), Carboxymethyl cellulose (CMC, MW: 240,000 g/mol), di-ammonium hydrogen phosphate ($(NH_4)_2HPO_4$), cobalt nitrate hexahydrate ($Co(NO_3)_2{\cdot}6H_2O$), calcium nitrate tetra-hydrate ($Ca(NO_3)_2$-·4H2O), and cobalt chloride hexahydrate ($CoCl_{2\cdot 6}H_2O$) were purchased from Sigma–Aldrich (USA). Acetone and acid acetic were purchased from Merck (Darmstadt, Germany). Dulbecco's Phosphate Buffer Saline (DPBS), Fetal Bovine Serum (FBS), Dulbecco's Modified Eagle Media (DMEM), Antibiotic– Antimycotic solution, Trypsin–EDTA, and MTT assay kit were obtained from Himedia (Mumbai, India).

2.2. Cobalt-doped hydroxyapatite synthesis

A wet chemical method based on salts' ammoniacal co-precipitation was applied to synthesize the cobalt-doped hydroxyapatite (CoHA). A proper amount of $Ca(NO_3)_2{\cdot}4H_2O$ was dissolved in 500 ml deionized (DI) water to obtain a 0.02 M solution and stirred at room temperature. Then, the cobalt sources ($CoCl_{2\cdot 6}H_2O$ and $Co(NO_3)_2{\cdot}6H_2O$) were added to the solution with the cobalt to calcium weight percentages of 10 %. In the next step, 200 ml of 0.03 M of $(NH_4)_2HPO_4$ solution was added to the Ca solution drop-wise at a rate of $\sim$ 2 ml/min. The pH of the solution was adjusted to 11 using NaOH 1 M and the solution was stirred for 4 h under vigorous magnetic stirring at 80 °C. Then, the slurry was aged at (30 ± 5 °C) for 24 h, following centrifugation and several washing steps of the precipitate with DI water. The obtained product was dried at 50 ± 5 °C for 24 h to obtain CoHAp powder.

2.3. Cobalt-doped hydroxyapatite characterization

The X-ray diffraction (XRD) analysis was conducted to assess the crystallinity of the prepared CoHA using a diffractometer (Philips XRD-PW1700) at the scan range of 20° – 60° 2θ with the step size of 2° (2θ)/min. FTIR spectroscopy was used to evaluate the functional groups of the synthesized CoHA based on the KBr pellet method over the scanning range of 400–4000 cm^{-1} using a Shimadzu/IR prestige 21 instrument.

2.4. Nanofibrous composite synthesis

The electrospinning technique was used to fabricate the nanofibrous nanocomposite. A solution containing 10 wt% PCL and 2 % wt.% CMC was prepared and stirred for 24 at 40 °C to obtain a homogenous and clear solution. Then, different concentrations CoHA (5, 10, and 15 wt% with respect to the dry mass of polymers) were added to the prepared solution, thoroughly sonicated, and stirred for 24 h. The prepared solution was converted to the nanofibrous nanocomposites

using an electrospinning apparatus with an applied voltage of 18 kV, feeding rate of 1 ml.min-1 and the tip to collector distance of 12 cm. The fabricated nanofibrous nanocomposites were treated with NaOH/EtOH (4:1) solution for 12 h.

2.5. Nanofibrous composite characterization

2.5.1. Morphology observation

The morphology of the prepared nanofibrous nanocomposite was evaluated using a scanning electron microscope (SEM, DSM 960A, Zeiss, Germany). The samples were coated with a thin layer of gold using a sputter-coater (Cressington 108 auto, UK) and imaged at the 20 kV accelerating voltage. The nanofiber's diameter was measured and calculated using the Image J software (1.47v, National Institute of Health, USA).

2.5.2. Water absorption assessment

The water absorption capacity of the prepared nanofibrous nanocomposite as the indication of their hydrophilic/hydrophobic nature was measured based weighing method. The scaffolds were soaked in DI water for 24 h and the water absorption percentage was measured using the following equation (Eq. (1)).

$$\text{Water absorption}\,(\%) = \left(\frac{\text{W1} - \text{W0}}{W0}\right) \times 100 \quad (1)$$

2.5.3. Mechanical strength measurement

The mechanical strength of the prepared nanofibrous mats was measured based on the tensile strength method and ASTM-D882 standard using a SANTAM (STM-20, Korea) universal testing machine. Rectangular strips of samples (90 mm × 5 mm) were cut and evaluated at a crosshead speed of 12.5 mm/min. The obtained load–displacement data was converted to stress–strain based on: Stress = Load/Area of cross section of specimen and Strain = Displacement/L(original length).

2.6. Hemolysis induction assessment

The hemolysis induced by the fabricated nanofibrous nanocomposites was measured quantitatively based on the American Society for Testing Materials (ASTMF 756–00, 2000) protocol. The scaffolds (10 mg) were incubated with 200 µL of fresh anticoagulated blood diluted with normal saline (1:2) for one h at 37 °C. Then, the incubated blood was centrifuged at 1500 rpm for 5 min at 4 °C and the absorbance of the supernatants was read at 545 nm using a microplate reader. Equation (2) was used to calculate the percentage of hemolysis induced by the samples.

$$\text{Hemolysis}\,(\%) = \left(\frac{Dt - Dnc}{Dpc - Dnc}\right) \times 100 \quad (2)$$

Where Dt was the absorbance of the samples, Dnc was the absorbance of the negative control (blood incubated with normal saline), and Dpc was the absorbance of the positive control (blood lysed with 0.1 M HCl).

2.7. Cell viability assessment

The proliferation/viability of L929 cells on the prepared nanofibrous nanocomposites was evaluated using the MTT assay method. The fabricated nanofibers were cut circulatory, put at the bottom of a 96-well plate, and sterilized by ethanol 70 % for two h and UV radiation for four h. The samples were washed three times with sterilized PBS (pH: 7.4) and incubated

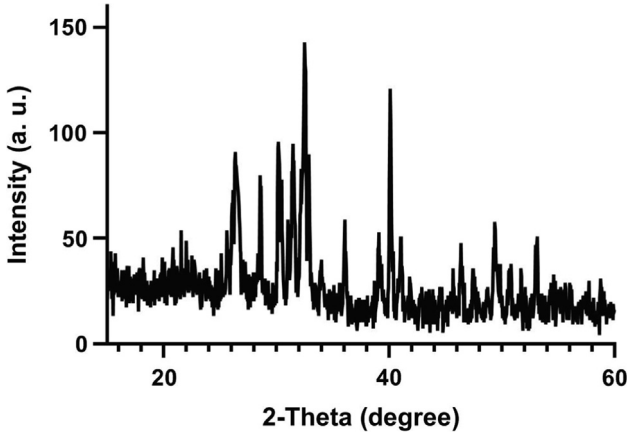

Fig. 2 XRD pattern of the synthesized Cobalt-doped HA crystals.

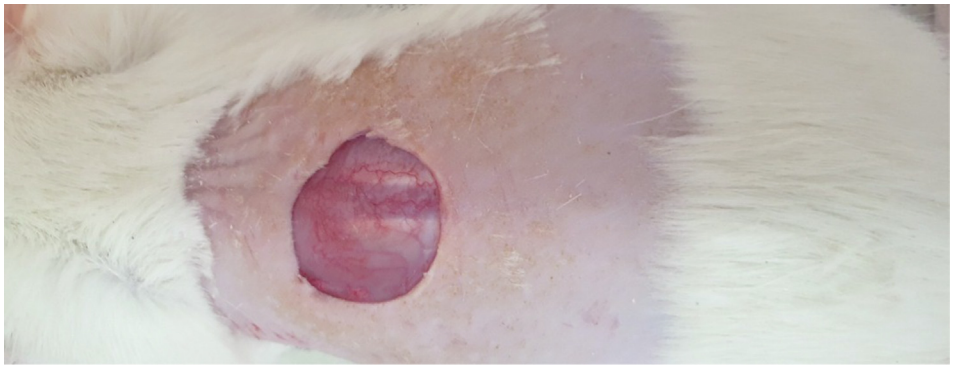

Fig. 1 The induced full-thickness wound (1.5 × 1.5 cm^2) on the back of the Wistar rat.

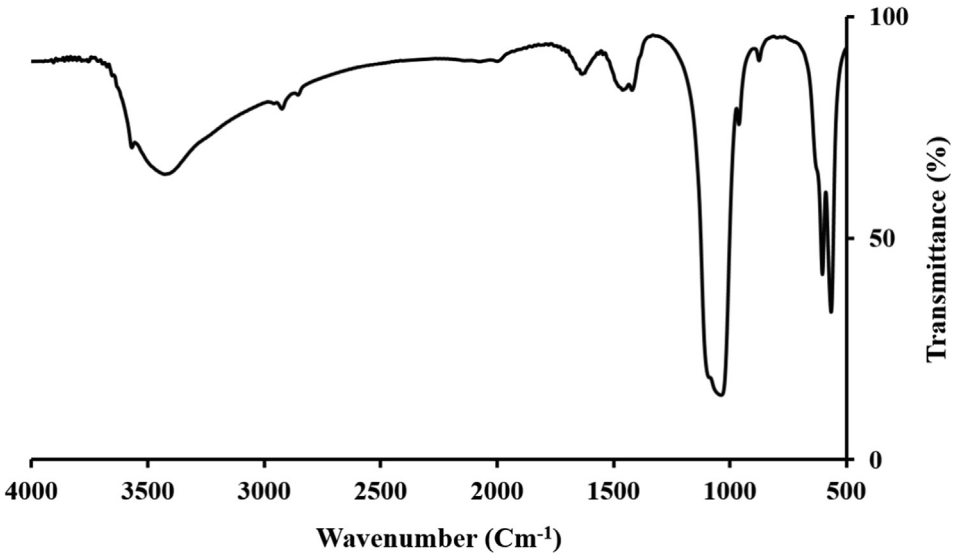

Fig. 3 FTIR specter of the synthesized Cobalt-doped HA crystals.

Table 1 FTIR characteristic bands of hydroxyapatite.

Type of bond	Wavenumber
ν_2 bending of the phosphate group	473 cm^{-1}
ν_3 stretching vibrations of the phosphate groups $(PO_4)^{3-}$	1035 cm^{-1} and 1095 cm^{-1}
ν_4 vibrational bands of the phosphate groups $(PO_4)^{3-}$	566, 633, and 603 cm^{-1}
hydroxyl group (OH^-) of HA and O—H stretching of the absorbed water	3450 cm^{-1} and 3572 cm^{-1}

with the complete cell culture medium for 24 h. The cells with the density of 5 × 104 cells/scaffold in 100 µL DMEM cell culture medium containing FBS 10 % and antibiotics-antimitotic were seeded on the nanofibers and incubated for 24, 48, and 72 h at 37 °C, 5 % CO_2 and 95 % humidity. After the incubation times, the culture medium was aspirated, the cells were washed with PBS and incubated with the 150 µL MTT salt for four h in a dark place. Then, 200 µL was added to the wells to dissolve the formed formazan crystals and the absorbance of samples was read at 540 nm using the microplate reader (Anthos 2020, Biochrom, Berlin, Germany). Equation (2) was used to calculate the proliferation percent.

$$\text{Cell proliferation}\,(\%) = \left(\frac{ODt}{ODc}\right) \times 100 \qquad (3)$$

Where ODt is the absorbance of the test and ODc is the absorbance of the control (cell cultured on tissue culture plastic).

2.8. In vivo wound healing evaluation

Animal studies were conducted to assess the wound healing efficacy of the prepared nanofibrous nanocomposites. The experiments were conducted according to the NIH guideline on thirty adult male Wistar rats (2 months old, weighing 200–220 g). All animal used procedures were carried out in accordance with the Regulations of Experimental Animal Administration. Intraperitoneal injection of a mixture of Xylazine (0.02 ml/10 g body weight) and Ketamine (0.04 ml/100 g body weight) was applied to induce general anesthesia and full-thickness excisional wound (1.50 × 1.50 cm^2) was applied on the back of rate (Fig. 1). The animals were randomly divided into five groups (six rats in each group) and treated with normal saline (The control), PCL/CMC, PCL/CMC/CoHA 5 %, PCL/CMC/CoHA 10 %, and PCL/CMC/CoHA 15 % nanocomposites. The healing process was monitored via macroscopic evaluation and calculating the wound closure percentage using Equation (3).

$$\text{Wound closure}\,(\%) = \left(1 - \frac{OOpenwoundareaDt}{Initialwoundarea}\right) \times 100 \qquad (4)$$

At 14 days post-treatment, a high dose of the anesthetic drugs (ketamine/Xylazine, 150/20 mg per kg) was injected to sacrifice the animals. The wound tissues were harvested, and fixed in paraformaldehyde (10 %, pH:7.26) for 48 h. The fixed tissues were blocked, sectioned, and stained with Hematoxylin and Eosin (H&E) staining.

3. Results and discussion

3.1. Cobalt-doped hydroxyapatite characteristics

A wet ammoniacal co-precipitation method was conducted to synthesis the Co-doped HA crystals. The XRD analysis showed that the synthesized exhibited the characteristic peaks of crystalline HAp ($Ca_{10}(PO_4)_6(OH)_2$) as indicated in the standard data sheet (JCPDS No. 09–0432) (Yang, 2009). The sharp peak located at around 26θ is related to the (002) plane of apatite crystal (Fig. 2). The peaks located at 40°, 47°, 50°, 52° and 53° 2θ are attributed to the crystal planes (310), (222), (213), (402) and (004) of HAp (Kulanthaivel, 2016).

FTIR spectroscopy was performed to assess the functional groups of the synthesized Cobalt-doped HA crystals. The results showed that the synthesized Cobalt-doped HA crystals exhibited the characteristic peaks of standard HA crystals (Fig. 3). The peak located at 473 cm^{-1} can be attributed to the ν_2 bending of the phosphate group. The peaks located at

1035 cm^{-1} and 1095 cm^{-1} are related to the ν_3 stretching vibrations of the phosphate groups $(PO_4)^{3-}$ (Yang, 2009). The peaks located at 566, 633, and 603 cm^{-1} are also related to the ν_4 vibrational bands of the phosphate groups $(PO_4)^{3-}$ (Han et al., 2009). The peaks located around 3450 cm^{-1} and 3572 cm^{-1} can be attributed to the hydroxyl group (OH^-) of Hap and O—H stretching of the absorbed water (Stojanović, 2009). The characteristic FTIR bands of HA crystals are collected in the Table 1.

3.2. Nanofibrous composite morphology

The morphology of the fabricated nanofibrous nanocomposites with different concentrations of Cobalt-doped HA crystals was imaged using SEM imaging, and the results are presented in Fig. 4. As shown in the images, the fabricated nanofibers are uniform and straight without any beads. Although, some deformations were observed in the nanofibrous nanocomposites containing the highest concentration (15 wt%) of crystals. As shown in the images, the presence of the synthesized Cobalt-doped HA crystals along the nanofibers is apparent and indicated with green arrows. The diameter of the fabricated nanofibers was measured using Image J software based on the SEM images. The results showed that the fabricated PCL/CMC, PCL/CMC/CoHA 5 %, PCL/CMC/CoHA 10 %, and PCL/CMC/CoHA 15 % have the diameter of 383 ± 50, 391 ± 84, 441 ± 65, and 495 ± 99 nm, respectively. It was observed that the incorporation and increasing the concentration of Cobalt-doped HA crystals increased the diameter of nanofibers, which was not statistically significant ($p < 0.1$).

The EDX elemental analysis was used to validate cobalt's presence further and discriminate its concentration difference in the prepared nanofibrous nanocomposites. The results are shown in Fig. 5. As shown in the images, there is an apparent difference between the cobalt content of the prepared nanofibrous nanocomposites.

The porosity of the fabricated nanofibrous composites was measured based on the liquid displacement method and the results are reported in Fig. 6. The results indicated that the fabricated nanofibrous composites have a porosity value in the

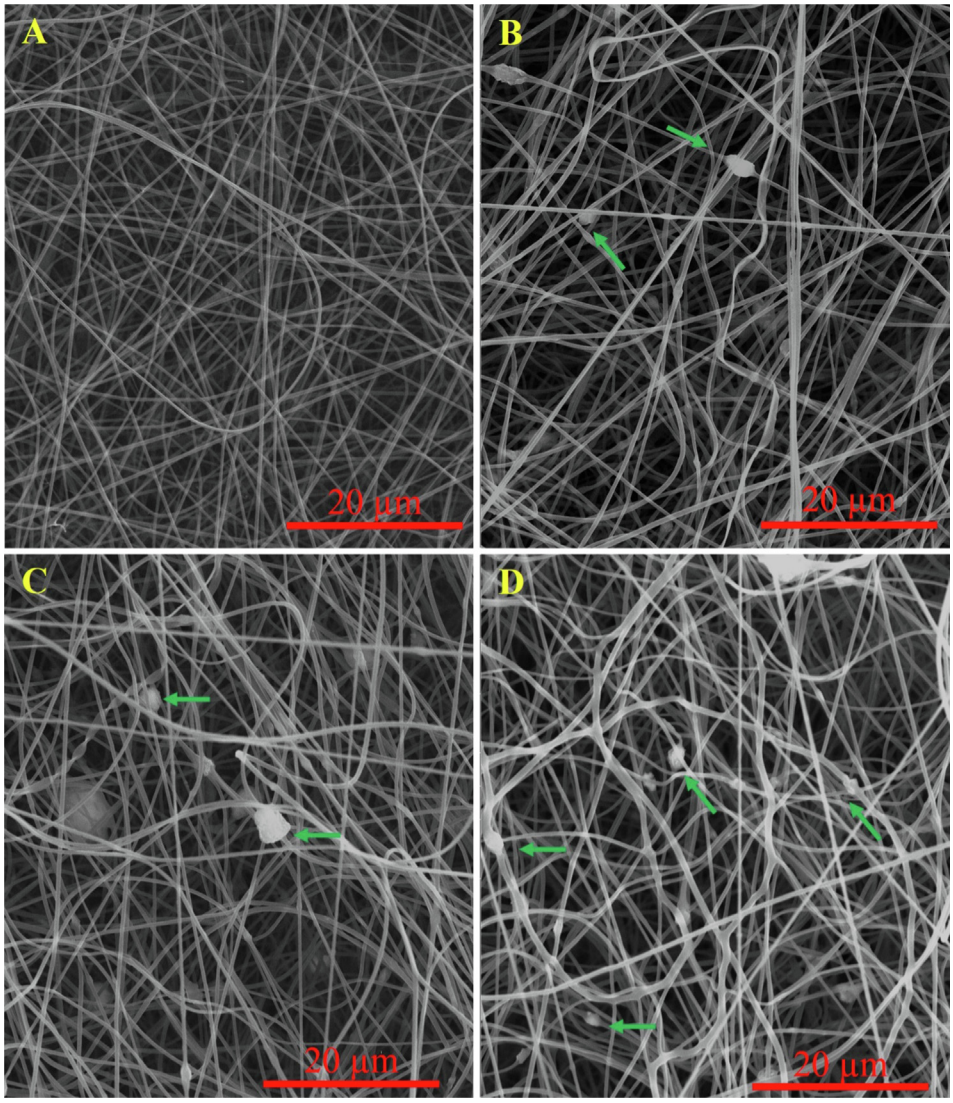

Fig. 4 SEM images of the fabricated nanofibrous composites containing 0 (A), 5 (B), 10 (C), and 15 wt% (D) Cobalt-doped HAp.

range from 40 to 55 %. Moreover, it was observed that increasing the concentration of the synthesized Cobalt-dope HAp did not significantly affect the porosity. Porosity is a key parameter for the wound dressing materials determining the gases and vapor exchange between the wound bead and the environment. Hartatiek et al. fabricated Poly(vinyl alcohol) (PVA)/Hydroxyapatite composite nanofibers and reported that the porosity of the composite was in the range of 62 to 74 % (Wuriantika, 2021).

It has been reported that, according to the wet wound healing hypothesis, wound healing goes better in a wet environment compared with a dry environment (Junker, 2013). The wet or moist wound healing process enhances the re-epithelialization process and reduces scar formation. Accordingly, preserving the wound healing wet is challenging in designing the wound dressing. Water absorption and retention are the ability of a wound dressing influencing the moisture of the wound bed. Moreover, optimum water absorption capacity is beneficial for absorption of the exudates secreted from the wound bed (Bao, 2020; Bishop, 2003). Water absorption capacity of the prepared nanofibrous nanocomposites was measured based on the gravimetric method. The results are reported in Fig. 7. The results showed that the water the absorption capacity of the nanofibrous nanocomposites were in the range of 32 to 63 %. Moreover, incorporation and increasing the concentration of Cobalt-doped HAp increased the water absorption capacity, which can be attributed to the highly hydrophilic nature of the Cobalt-doped HAp (Lowe, 2016).

3.3. Nanofibrous composite mechanical strength

A proper wound dressing must possess acceptable mechanical strength to be adapted to body movements. The mechanical strength of the prepared nanofibrous nanocomposites was measured based on the tensile strength assessment method

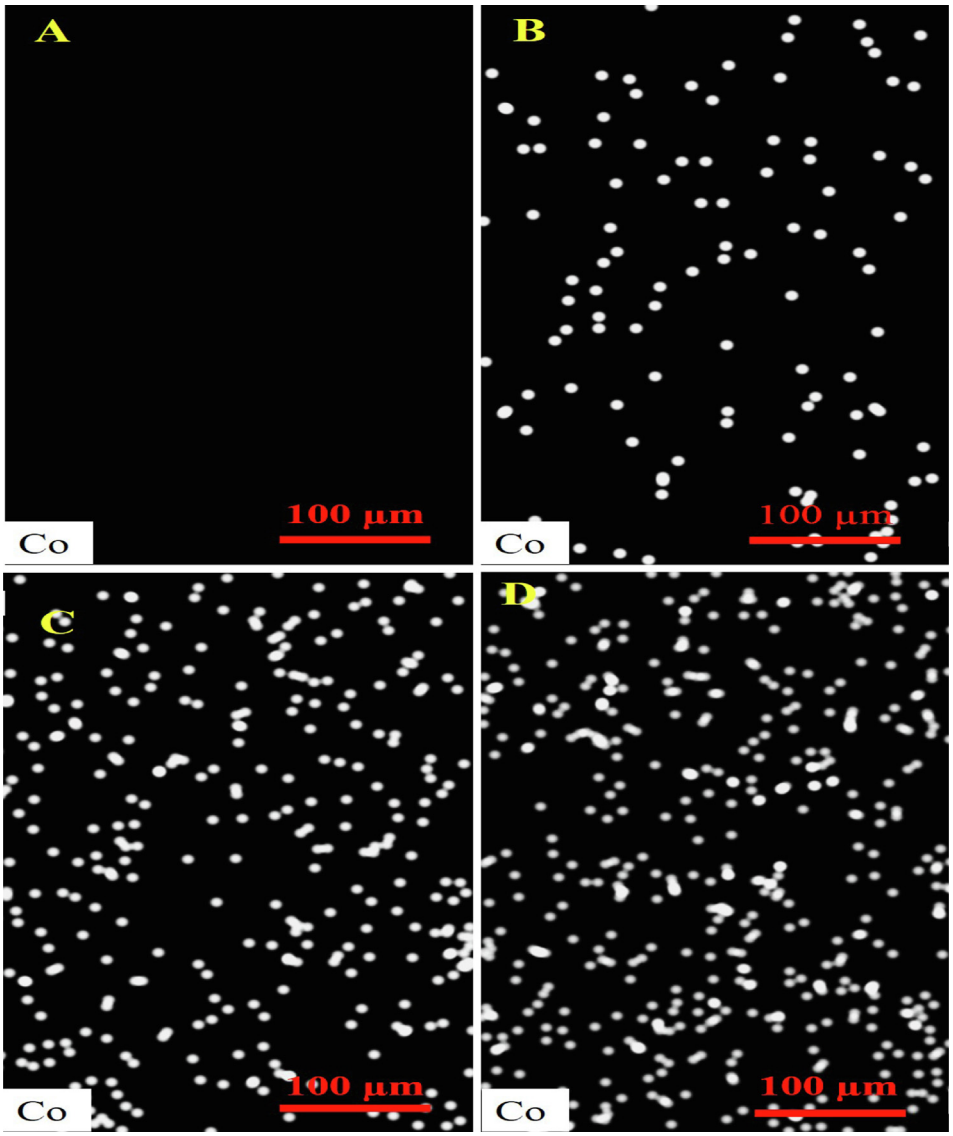

Fig. 5 EDX elemental analysis of the fabricated nanofibrous composites containing 0 (A), 5 (B), 10 (C), and 15 wt% (D) Cobalt-doped HAp.

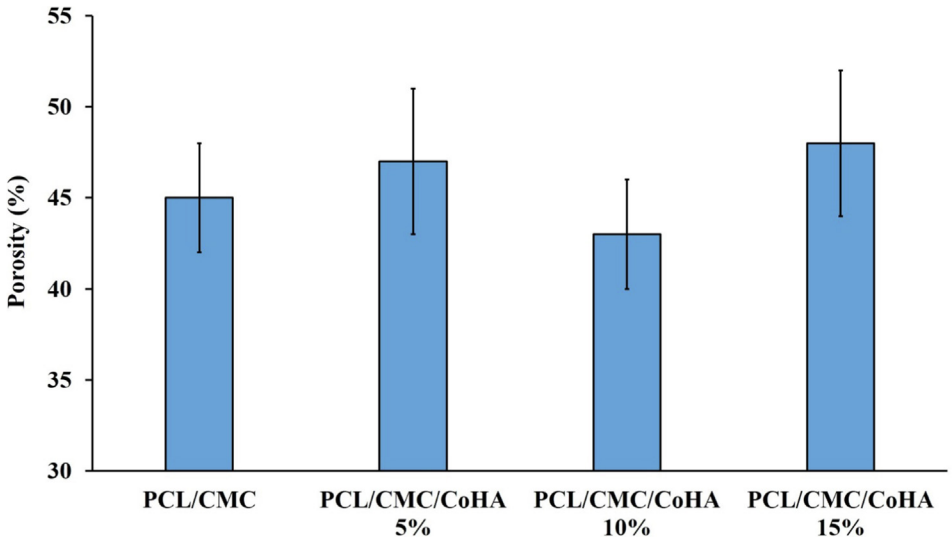

Fig. 6 Porosity of the fabricated nanofibrous composites measured based on the liquid displacement method.

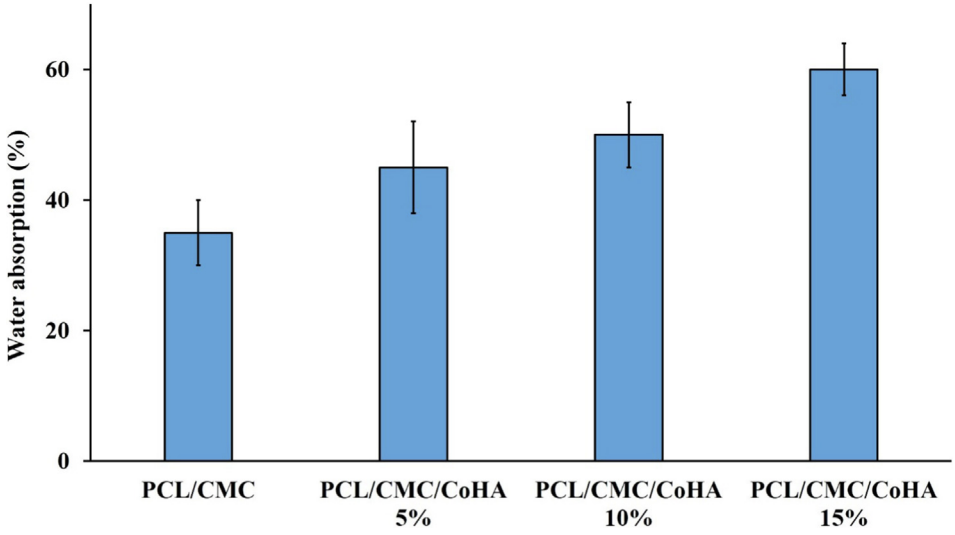

Fig. 7 Water absorption capacity of the prepared nanofibrous nanocomposites.

and the results are reported in Fig. 8. The results showed that the incorporation of Cobalt-doped HAp increased the mechanical strength of the nanocomposites. The highest mechanical strength was obtained using 15 wt% HAp. Hartatiek et al. also reported that the mechanical strength of PVA nanofibers was increased with the addition of HAp (Wuriantika, 2021).

3.4. Hemocompatibility

It is necessary to evaluate the hemocompatibility of the fabricated wound dressing. Hemolysis induced by the fabricated nanofibrous nanocomposites was measured using UV–vis spectroscopy to indicate hemocompatibility. As shown in Table 2, the prepared nanofibrous nanocomposites induced hemolysis lower than 10 %, indicating the hemocompatibility of the structures. Moreover, the effect of incorporating different amount of CoHA on the observed hemolysis was negligible and statistically not significant. Kulanthaivel et al. fabricated Cobalt-doped proangiogenic HAp as the bone tissue engineering structure and reported that the fabricated bioceramics induced negligible hemolysis and were hemocompatible (Kulanthaivel, 2016).

3.5. Cell viability results

The viability and proliferation of L929 cells on the fabricated nanofibrous nanocomposites were evaluated using the MTT assay kit. The MTT assay measures the metabolic activity of the cells and it can be related to the viability and proliferation of the cells. The results showed that the viability of the cells on the tissue culture plastic (TCP) was higher than the nanocomposites. This can be related to the fact that 24 h is a short time for adapting the cells with nanocomposites. On the other hand, at 48 and 72 post cell seeding, the proliferation of the cells on the nanocomposites was higher than in the control group. The

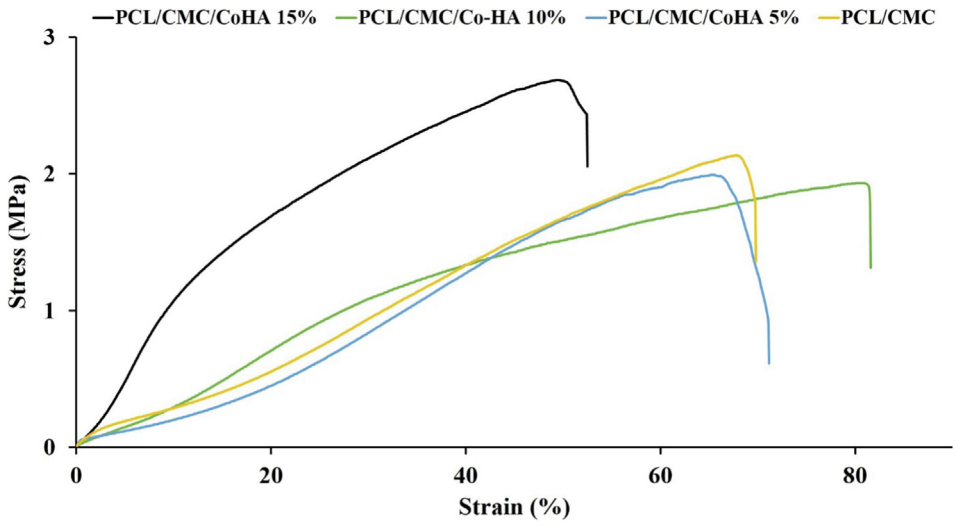

Fig. 8 Strain-Stress curve of the fabricated nanofibrous nanocomposites.

Table 2 Hemolysis percent induced by the fabricated nanofibrous nanocomposites.

Samples	Hemolysis (%)
Positive control	100
PCL/CMC	7.1 ± 2.0
PCL/CMC/CoHA 5 %	5.4 ± 1.4
PCL/CMC/CoHA 10 %	6.2 ± 1.1
PCL/CMC/CoHA 15 %	7.9 ± 2.3

highest cell proliferation was obtained with PCL/CMC/CoHA at 10 %, and the higher concentration of Cobalt-doped HAp suppressed the cell proliferation (Fig. 9).

3.6. In vivo wound healing findings

The wound healing efficacy of the fabricated nanofibrous nanocomposites was investigated in an animal model. The full-thickness wound model was induced on the back of rates and dressed with the fabricated nanofibrous nanocomposites and the healing process was monitored for 14 days based on the macroscopic evaluation (wound closure percentage) (Fig. 10) and at the end of the treatment based on the microscopic evaluation (histopathological assessment). The wound closure measurement revealed that the negative control could not contract completely, resulting in 80 ± 5 % wound closure. The highest wound closure percentage (95 ± 4 %) was obtained under treatment with PCL/CMC/CoHA 10 %, while the PCL/CMC/CoHA 15 % resulted in 85 ± 4 % wound closure. These observations illustrated that untreated wounds could not be fully contracted and required proper treatment,

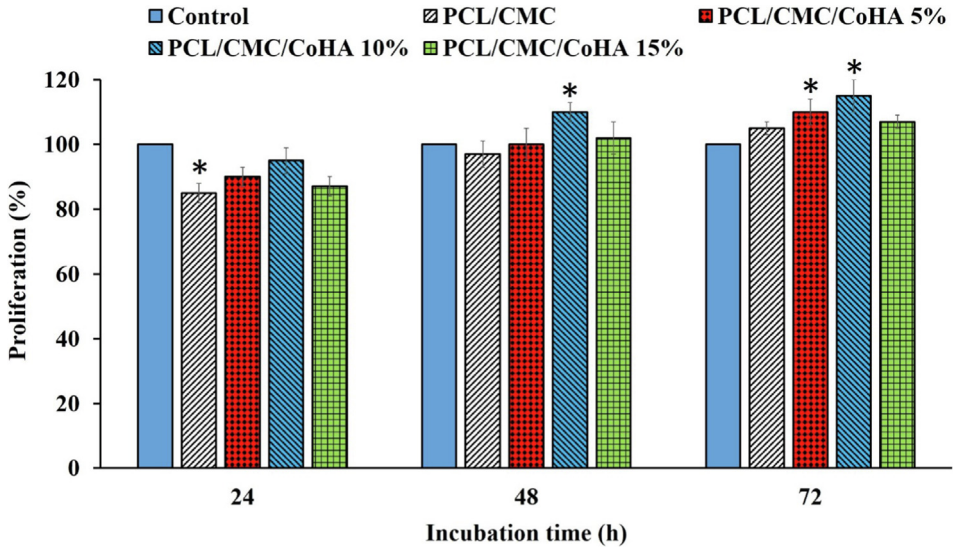

Fig. 9 Proliferation of L929 cells on the fabricated nanofibrous nanocomposites measured by the MTT assay kit. Control: Tissue Culture Plate (TCP). Data represented as mean ± SD, n = 3. *p < 0.05 (obtained by one-way ANOVA).

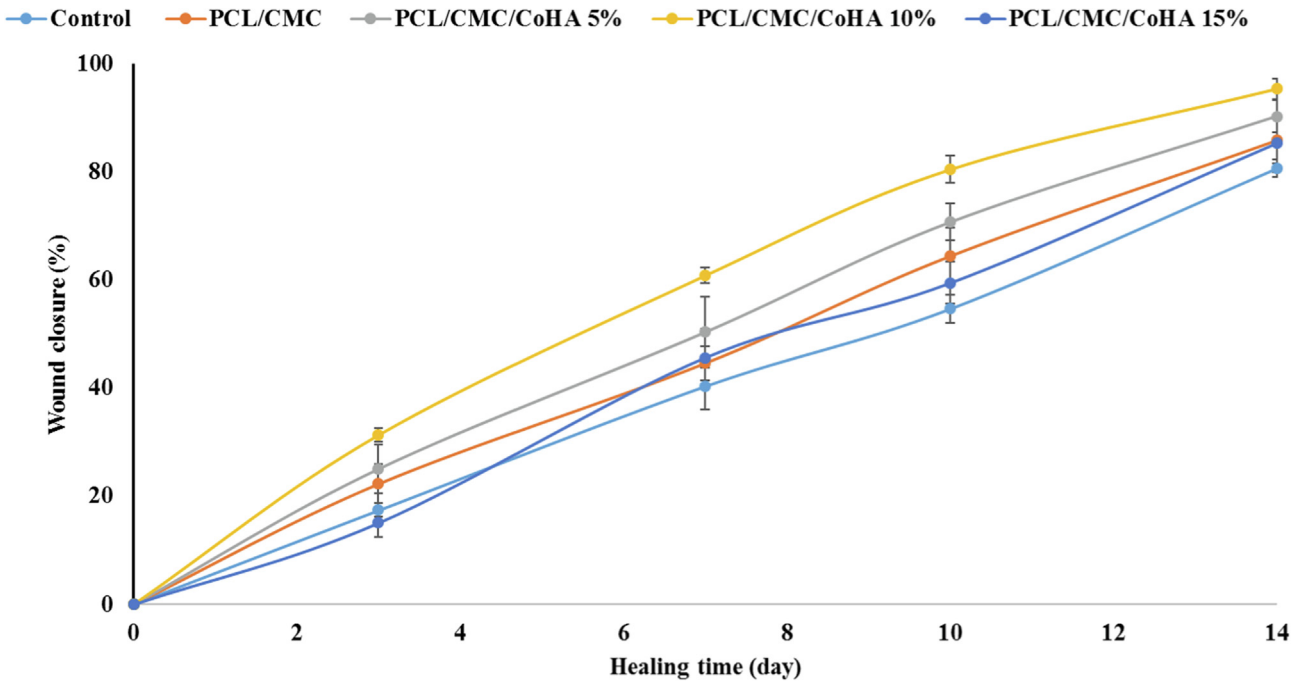

Fig. 10 Wound closure measurement results of the full thickness wound treated with the fabricated nanofibrous wound dressings.

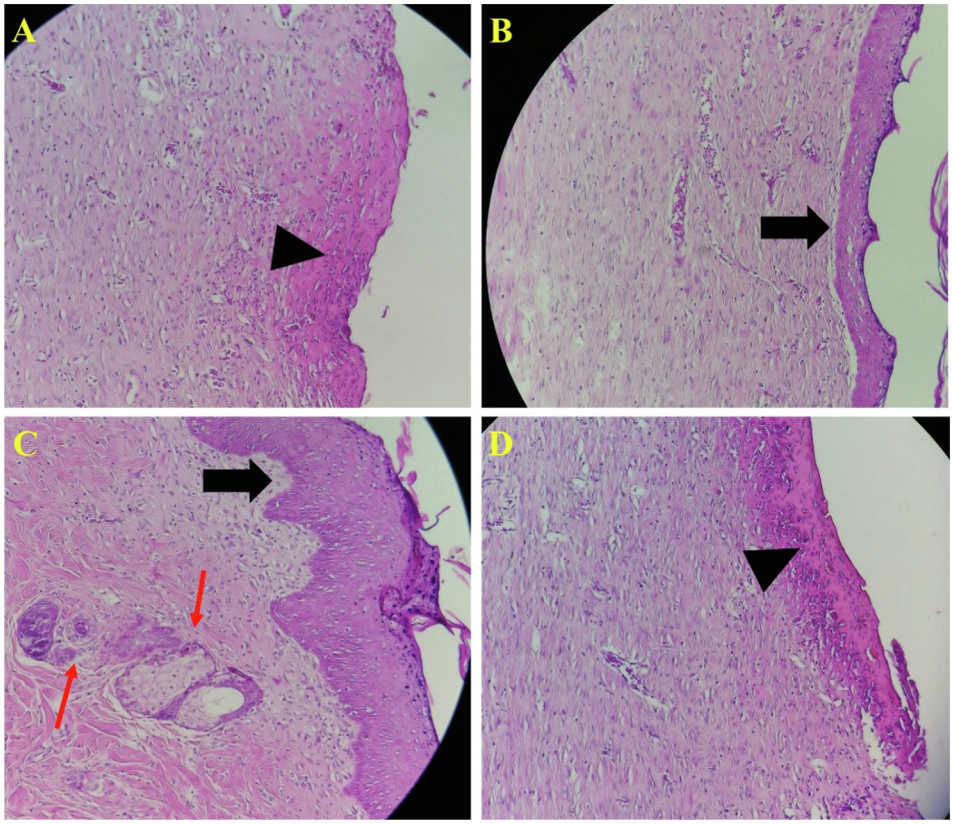

Fig. 11 Histopathology evaluation of wounds stained with Hematoxylin and eosin (H&E) staining. (A) negative control group (without treatment), (B) wound treated with PCL/CMC/CoHA 5%, (C) wound treated with PCL/CMC/CoHA 10%, and (D) wound treated with PCL/CMC/CoHA 15%. The treatment using PCL/CMC/CoHA 15% resulted in healing outcomes like the negative control group, unformed epidermal layer, crusty scab coverage and PMNs infiltration.

which agrees with the previous studies reporting that 21 days require complete wound contraction without any treatments (Winter, 1963; Maalej, 2014).

Histopathology was conducted using the H&E staining to further evaluate the wound healing process under treatment with the fabricated nanofibrous nanocomposites and the results are presented in Fig. 11. The results revealed that in the negative control group, the epidermal layer had not been formed and the wound surface is covered with a crusty scab (Fig. 11 A, arrowhead). Moreover, this group's infiltration of polymorphonuclear inflammatory cells (PMNs) is dominant. It was observed that the wound treated with PCL/CMC/CoHA 5 % resulted in the partial formation of the epidermal layer (Fig. 11 B, thick arrow), although the PMNs cells infiltration was apparent. The best treatment outcome was obtained under treatment with PCL/CMC/CoHA 10 % which the epidermal layer was formed and wrinkled (Fig. 11 C, thick arrow). Moreover, sebaceous glands and hair follicles are observed in this group, indicating the most resemblance to normal skin. On the other hand, the treatment using PCL/CMC/CoHA 15 % resulted in healing outcomes like the negative control group, unformed epidermal layer, crusty scab coverage and PMNs infiltration. Various studies applied calcium phosphate-based bioceramics to improve wound healing process. Zhou et al. fabricated collage nanofibers containing bioactive glass ceramics as wound healing materials. They reported that the fabricated nanofibers exhibited physicochemical properties suitable for wound healing and management. They showed that the wound healing process was accelerated upon applying the nanofibers (Zhou, 2017). Ashraf and colleagues synthesized aluminum/vanadate ions doped-HA crystals and incorporated the crystals in PCL nanofibers. They reported that the nanofibers were cytocompatible and can be applied as the wound dressing materisl (Ashraf, 2021).

4. Conclusion

Wound healing is a complicated and multi-step process; without treatment, skin cannot heal properly in a reasonable time. Accordingly, sophisticated wound healing/dressing materials are required to promote wound healing process. In the current study, we fabricated nanofibrous nanocomposites based on PCL and CMC polymers containing various concentrations of Cobalt-doped HAp as the wound dressing materials. The fabricated Cobalt-doped HAp and nanofibrous nanocomposites were thoroughly characterized and observed that they possess beneficial characteristics. The in vitro biological properties evaluations indicated that the fabricated nanofibrous nanocomposites were hemocompatible and biocompatible in the optimum condition. The animal studies also revealed that the nanofibrous nanocomposites promoted the wound healing process and the best healing outcomes were observed under treatment with PCL/CMC/CoHAp nanocomposite. In conclusion, this study showed that the combination of Cobalt-doped HAp with nanofibers of PCL/CMC results in bioactive wound dressing applicable for wound healing management.

Declaration of Competing Interest

The authors declare that they have no known competing financial interests or personal relationships that could have appeared to influence the work reported in this paper.

References

Abdelrahman, T., Newton, H., 2011. Wound dressings: principles and practice. Surgery (Oxford) 29 (10), 491–495.

Ansari, S.M. et al, 2018. Controlled surface/interface structure and spin enabled superior properties and biocompatibility of cobalt ferrite nanoparticles. Appl. Surf. Sci. 459, 788–801.

Asadi, N. et al, 2021. Multifunctional hydrogels for wound healing: Special focus on biomacromolecular based hydrogels. Int. J. Biol. Macromol. 170, 728–750.

Ashraf, S. et al, 2021. Nanofibers of polycaprolactone containing hydroxyapatite doped with aluminum/vanadate ions for wound healing applications. New J. Chem. 45 (48), 22610–22620.

Bao, F. et al, 2020. Bioactive Self-Pumping Composite Wound Dressings with Micropore Array Modified Janus Membrane for Enhanced Diabetic Wound Healing. Adv. Funct. Mater. 30 (49), 2005422.

Beladi, F., Saber-Samandari, S., Saber-Samandari, S., 2017. Cellular compatibility of nanocomposite scaffolds based on hydroxyapatite entrapped in cellulose network for bone repair. Mater. Sci. Eng., C 75, 385–392.

Bishop, S. et al, 2003. Importance of moisture balance at the wound-dressing interface. Journal of wound care 12 (4), 125–128.

Braiman-Wiksman, L. et al, 2007. Novel insights into wound healing sequence of events. Toxicologic pathology 35 (6), 767–779.

Dlugosz, A.A., Yuspa, S.H., 1994. Protein kinase C regulates keratinocyte transglutaminase (TGK) gene expression in cultured primary mouse epidermal keratinocytes induced to terminally differentiate by calcium. J, Invest. Dermatol. 102 (4), 409–414.

Doozandeh, Z., Saber-Samandari, S., Khandan, A., 2020. Preparation of novel Arabic gum-C6H9NO biopolymer as a bedsore for wound care application. Acta Medica Iranica, 520–530.

Farazin, A. et al, 2021. A Review on Polymeric Wound Dress for the Treatment of Burns and Diabetic Wounds. International Journal of Basic Science in Medicine 6 (2), 44–50.

Han, Y., Wang, X., Li, S., 2009. A simple route to prepare stable hydroxyapatite nanoparticles suspension. J. Nanopart. Res. 11 (5), 1235–1240.

Han, S.-K., 2016. Interactive wound dressings. In: Innovations and Advances in Wound Healing. Springer, pp. 39–61.

Hosgood, G., 2006. Stages of wound healing and their clinical relevance. Veterinary Clinics: Small Animal Practice 36 (4), 667–685.

Junker, J.P. et al, 2013. Clinical impact upon wound healing and inflammation in moist, wet, and dry environments. Advances in wound care 2 (7), 348–356.

Kawai, K. et al, 2011. Calcium-based nanoparticles accelerate skin wound healing. PloS one 6 (11), e27106.

Klein, S. et al, 2018. Enhanced in vitro biocompatibility and water dispersibility of magnetite and cobalt ferrite nanoparticles employed as ROS formation enhancer in radiation cancer therapy. Small 14 (21), 1704111.

Kulanthaivel, S. et al, 2016. Cobalt doped proangiogenic hydroxyapatite for bone tissue engineering application. Mater. Sci. Eng., C 58, 648–658.

Lansdown, A.B., 2002. Calcium: a potential central regulator in wound healing in the skin. Wound repair and regeneration 10 (5), 271–285.

Lee, S.H. et al, 1998. Iontophoresis itself on hairless mouse skin induces the loss of the epidermal calcium gradient without skin barrier impairment. J, Invest. Dermatol. 111 (1), 39–43.

Lickmichand, M. et al, 2019. In vitro biocompatibility and hyperthermia studies on synthesized cobalt ferrite nanoparticles encapsulated with polyethylene glycol for biomedical applications. Mater. Today:. Proc. 15, 252–261.

Lowe, B. et al, 2016. Preparation and characterization of chitosan-natural nano hydroxyapatite-fucoidan nanocomposites for bone tissue engineering. Int. J. Biol. Macromol. 93, 1479–1487.

Maalej, H. et al, 2014. Rhelogical, dermal wound healing and in vitro antioxidant properties of exopolysaccharide hydrogel from Pseudomonas stutzeri AS22. Colloids Surf. BBiointerfaces 123, 814–824.

Magee, A.I., Lytton, N.A., Watt, F.M., 1987. Calcium-induced changes in cytoskeleton and motility of cultured human keratinocytes. Exp. Cell Res. 172 (1), 43–53.

Maver, T. et al, 2015. Functional wound dressing materials with highly tunable drug release properties. RSC Adv. 5 (95), 77873–77884.

Mohammadi, Z. et al, 2019. The effect of chrysin–curcumin-loaded nanofibres on the wound-healing process in male rats. Artif. Cells Nanomed. Biotechnol. 47 (1), 1642–1652.

Raisi, A. et al, 2020. A soft tissue fabricated using a freeze-drying technique with carboxymethyl chitosan and nanoparticles for promoting effects on wound healing. Journal of Nanoanalysis 7 (4), 262–274.

Rajalekshmy, G., Rekha, M., 2021. Strontium ion cross-linked alginate-g-poly (PEGMA) xerogels for wound healing applications: in vitro studies. Carbohydr. Polym. 251, 117119.

Rawat, A., Bhatt, G.K., Kothiyal, P., 2016. Review on transdermal drug delivery system. Indo Am J Pharm Sci 3, 423–428.

Saber-Samandari, S. et al, 2018. The role of titanium dioxide on the morphology, microstructure, and bioactivity of grafted cellulose/hydroxyapatite nanocomposites for a potential application in bone repair. Int. J. Biol. Macromol. 106, 481–488.

Stojanović, Z. et al, 2009. Hydrothermal synthesis of nanosized pure and cobalt-exchanged hydroxyapatite. Mater. Manuf. Processes 24 (10–11), 1096–1103.

Trump, B.F. et al, 1984. Cell calcium, cell injury and cell death. Environ. Health Perspect. 57, 281–287.

Unnithan, A.R. et al, 2012. Wound-dressing materials with antibacterial activity from electrospun polyurethane–dextran nanofiber mats containing ciprofloxacin HCl. Carbohydr. Polym. 90 (4), 1786–1793.

Venus, M., Waterman, J., McNab, I., 2010. Basic physiology of the skin. Surgery (Oxford) 28 (10), 469–472.

Weller, C., Sussman, G., 2006. Wound dressings update. J. Pharm. Pract. Res. 36 (4), 318–324.

Winter, G.D., 1963. Effect of air exposure and occlusion on experimental human skin wounds. Nature 200 (4904), 378–379.

Wuriantika, M. et al, 2021. Nanostructure, porosity and tensile strength of PVA/Hydroxyapatite composite nanofiber for bone tissue engineering. Mater. Today:. Proc. 44, 3203–3206.

Yang, C. et al, 2009. Synthesis and characterization of Eu-doped hydroxyapatite through a microwave assisted microemulsion process. Solid State Sci. 11 (11), 1923–1928.

Yusof, N.L.B.M. et al, 2003. Flexible chitin films as potential wound-dressing materials: Wound model studies. Journal of Biomedical Materials Research Part A: An Official Journal of The Society for Biomaterials, The Japanese Society for Biomaterials, and The Australian Society for Biomaterials and the Korean Society for Biomaterials 66 (2), 224–232.

Zhou, T. et al, 2017. Multifunctional and biomimetic fish collagen/bioactive glass nanofibers: Fabrication, antibacterial activity and inducing skin regeneration in vitro and in vivo. Int. J. Nanomed. 12, 3495.